OPEN

# Diagnostic Capability of 3D Peripapillary Retinal Volume for Glaucoma Using Optical Coherence Tomography Customized Software

*Yingna Liu, MD,*† Firas Jassim, PhD,*‡ Boy Braaf, PhD,*§*
*Ziad Khoueir, MD,*‡‖ Linda Yi-Chieh Poon, MD,*‡¶*
*Geulah S. Ben-David, MD,*‡# Georgia Papadogeorgou, PhD,***
*Edem Tsikata, PhD,*‡ Huseyin Simavli, MD,*‡†† Christian Que, MD,*‡‡‡*
*Ramon Lee, MD,*‡§§ Eric Shieh, MD,*‡‖‖ Benjamin J. Vakoc, PhD,*§*
*Brett E. Bouma, PhD,*§ Johannes F. de Boer, PhD,¶¶##*
*and Teresa C. Chen, MD*‡*

Received for publication July 27, 2018; accepted May 5, 2019.

From the *Harvard Medical School; ‡Department of Ophthalmology, Glaucoma Service, Massachusetts Eye, and Ear Infirmary; §Wellman Center for Photomedicine, Massachusetts General Hospital; **Department of Biostatistics, Harvard T.H. Chan School of Public Health, Boston, MA; ‖Beirut Eye and ENT Specialist Hospital, Saint-Joseph University Medical School, Beirut, Lebanon; ¶Department of Ophthalmology, Kaohsiung Chang Gung Memorial Hospital, Chang Gung University College of Medicine, Kaohsiung, Taiwan; #Sackler School of Medicine, Tel Aviv University, Tel Aviv, Israel; ††Department of Ophthalmology, Pamukkale University, School of Medicine, Denizli, Turkey; ‡‡University of the East Ramon Magsaysay Memorial Medical Center, Quezon City, Philippines; †Department of Ophthalmology, University of California, San Francisco, San Francisco; §§Roski Eye Institute, University of Southern California; ‖‖Jules Stein Eye Institute, University of California, Los Angeles, Los Angeles, CA; ¶¶Department of Ophthalmology, Vrije Universiteit; and ##Department of Physics and Astronomy, LaserLaB Amsterdam, Vrije Universiteit, Amsterdam, The Netherlands.

T.C.C. has received funding from American Glaucoma Society Mid-Career Award, Massachusetts Lions Eye Fund, Harvard Catalyst Grant, National Institutes of Health Award #UL 1RR 025758, Fidelity Charitable Fund (Harvard University). H.S. is supported by TUBITAK (The Scientific and Technological Council of Turkey) 2219. B.B., B.J.V., and B.E.B. received funding from the Center for Biomedical OCT Research and Translation through grant number P41EB015903, awarded by the National Institute of Biomedical Imaging and Bioengineering of the National Institutes of Health (Bethesda, MD). B.J.V. is further supported by Alcon.

Disclosure: J.F.d.B. has the following disclosures: Harvard Medical School Center for Biomedical OCT Research and Translation Scientific Advisory Board Chair; Licenses to NIDEK Inc., Fremont, CA; Terumo Corporation, Tokyo, Japan; Heidelberg Engineering GmbH, Germany; and Ninepoint Medical, Bedford, MA. B.J.V. has the following disclosures: Licenses to Terumo Corporation, Tokyo, Japan, and Ninepoint Medical, Bedford, MA. B.E.B. has the following disclosures: Licenses to NIDEK Inc., Fremont, CA; Terumo Corporation, Tokyo, Japan, Ninepoint Medical, Bedford, MA and Heidelberg Engineering GmbH, Germany. The remaining authors declare no conflict of interest.

Reprints: Teresa C. Chen, MD, Massachusetts Eye and Ear Infirmary, Glaucoma Service, 243 Charles Street, Boston, MA 02114 (e-mail: teresa_chen@meei.harvard.edu).

Supplemental Digital Content is available for this article. Direct URL citations appear in the printed text and are provided in the HTML and PDF versions of this article on the journal's website, www.glaucomajournal.com.



DOI: 10.1097/IJG.0000000000001291

**Précis:** The diagnostic capability of peripapillary retinal volume is similar to peripapillary retinal nerve fiber layer thickness for diagnosing glaucoma, but with fewer artifacts.

**Purpose:** To compare the diagnostic capability of 3-dimensional peripapillary retinal volume (RV) versus 2-dimensional peripapillary retinal nerve fiber layer (RNFL) thickness for open-angle glaucoma.

**Patients and Methods:** A retrospective cross-sectional analysis was conducted. A total of 180 subjects (113 open-angle glaucoma, 67 normal participants) had spectral domain optical coherence tomography volume scans and RNFL thickness measurements. Peripapillary RV values were calculated using a custom-designed program with 4 circumpapillary annuli (CA): CA1 had circle diameters of 2.5 and 3.5 mm; CA2, 3 and 4 mm; CA3, 3.5 and 4.5 mm; and CA4, 4 and 5 mm. Area under the receiver operating characteristic curves were calculated for global, quadrant, and octant regions for RV (CA1 to CA4) and RNFL thickness. Pairwise comparisons were conducted. Artifacts rates were determined.

**Results:** Mean age was $62.7 \pm 15.4$ years, and 47.8% (86/180) were male. Among RV measurements, best diagnostic performances were for the smallest 2 annuli for inferior RV (CA1: 0.964, CA2: 0.955). Of the 4 annuli, CA1 had the highest diagnostic performance. Of specific regions, the inferior RV quadrant had the highest performance across CA1 to CA4. Peripapillary RV had similar diagnostic capability compared with RNFL thickness ($P > 0.05$). The artifact rate per B-scan for RV was 6.0%, which was significantly lower compared with 2-dimensional RNFL thickness in the same patient population (32.2%, $P < 0.0001$).

**Conclusions:** The diagnostic capability of RV is similar to RNFL thickness for perimetric open-angle glaucoma, but RV had fewer artifacts compared with RNFL thickness.

**Key Words:** open-angle glaucoma, optical coherence tomography, retinal volume

(*J Glaucoma* 2019;28:708–717)

Glaucoma is the leading cause of irreversible blindness worldwide,[1] and among populations of European and African descent, open-angle glaucoma (OAG) is the most common type.[1,2] Although initially asymptomatic, OAG may eventually progress to irreversible blindness. As timely initiation of treatment can be vision saving,[3] a reliable

diagnostic tool for OAG has important public health implications.

Retinal nerve fiber layer (RNFL) thickness, the thinning of which is a strong indicator of glaucoma,[4–7] is a parameter that can be measured by spectral domain (SD) optical coherence tomography (OCT) tool. The utility of RNFL thickness measurements, however, is limited by a high rate of artifacts. As much as 19.9%[8] to 46.3%[9] of SD-OCT RNFL scans have artifacts, including RNFL segmentation errors, decentration, poor signal, cut edge, motion artifacts, and patient pathology related errors including epiretinal membrane, peripapillary atrophy, and myelinated nerve fiber layer related artifacts. Furthermore, RNFL thinning can be seen in eye pathologies other than glaucoma.[10–16] Overall, the resulting rate of a false-positive glaucoma diagnosis when using Spectralis OCT's RNFL thickness measurement and overall classification color coding (red for glaucoma, yellow for maybe glaucoma, and green for normal) has been reported to be around 18%.[17]

Unlike the posterior RNFL border, which decreases in reflectivity with glaucoma in the setting of RNFL thinning,[18,19] the posterior retina border does not and therefore may be associated with fewer segmentation errors and artifacts.[20,21] Therefore, our group has previously shown that retinal thickness (RT) measurements from 3-dimensional (3D) volume scans, which were determined by centering the Early Treatment Diabetic Retinopathy Study (ETDRS) circular grid over the optic nerve, had the same or better diagnostic capability compared with peripapillary RNFL thickness but with fewer segmentation errors.[20,22] In contrast to peripapillary RT measurements, peripapillary retinal volume (RV) measurements have the advantage of offering more comprehensive 3D information, and therefore, may detect more subtle focal changes in the overall anatomy over time. Recently, our group showed that peripapillary RV measurements using ETDRS circular grids also had excellent diagnostic capability and significantly lower artifact rates compared with RNFL thickness.[22] Past RV studies have otherwise focused on retinal diseases, and macular RV has previously been studied in the context of wet macular degeneration and retinoschisis.[23,24] Because past RT and RV studies have used diabetic ETDRS software and have focused on the macular region for retinal diseases, this study will focus on analysis of the peripapillary region using software customized for glaucoma diagnosis. On the basis of these promising results,[20,22] we developed new software with adjustable annular sizes, different from regions on the ETDRS grid, to specifically capture glaucomatous peripapillary changes. We hypothesize that 3D peripapillary RV measurements from Spectralis OCT scans, using customized annular sizes, have equal or better diagnostic capabilities for glaucoma compared with the traditional 2-dimensional (2D) peripapillary RNFL thickness measurements.

## PATIENTS AND METHODS

### Participants and Eye Examinations

This is a retrospective cross-sectional study. The Massachusetts Eye and Ear Infirmary (MEEI) Institutional Review Board prospective approval for research involving human subjects was obtained. All participants were recruited from the Glaucoma Service at the MEEI between January 1, 2009, and July 31, 2014, as a part of the longitudinal Spectral Domain OCT in Glaucoma (SIG) study. Informed consent was obtained from all subjects in adherence to HIPAA, the tenets of the Declaration of Helsinki and the Health Insurance Portability and Accountability Act.

Details of the study methods have been described elsewhere.[20] Briefly, all subjects underwent a complete eye examination by a glaucoma fellowship-trained ophthalmologist (T.C.C). Patients were included if they fulfilled all of the inclusion criteria: (1) a spherical equivalent between −5.0 and +5.0 D, (2) a best-corrected visual acuity of 20/40 or better, and (3) reliable visual field (VF) with 33% or fewer fixation losses, 20% or less false-positive results, and 20% or less false-negative results. Exclusion criteria were: (1) discernible anterior segment dysgenesis, (2) corneal scarring or opacities, (3) severe nonproliferative or proliferative diabetic retinopathy, (4) VF loss attributable to a nonglaucoma condition, and (5) a dilated pupil diameter of <2 mm. Patients were diagnosed with OAG if they had characteristic changes of the optic nerve head (ONH) with corresponding VF defects (such as nasal steps, arcuate or Bjerrum scotoma, paracentral scotoma, altitudinal defect), as determined by a glaucoma specialist (T.C.C.).[4] This study included patients with primary OAG, pigmentary glaucoma, pseudoexfoliation glaucoma, and normal tension glaucoma. Normal subjects were those with only mild cataracts or with a history of cataract surgery.[25] Only the scans of OAG and normal subjects were analyzed. If both eyes were eligible, one eye was selected randomly.

### Spectralis OCT Peripapillary RV Scans and RNFL Thickness Scans

After pupillary dilation, all SD-OCT volume scan imaging was performed with the Spectralis OCT machine with the automatic real time (ART) function activated (HRA/Spectralis software version 5.4.8.0).[20,26,27] The ART function was combined with the eye-tracking system to acquire multiple frames at the same scan location. Volume scans were obtained with a 20×20-degree field centered on the ONH. 193 sections were taken with high-speed rate and 3 frames for ART. The average RNFL thickness was measured by OCT Spectralis using the standard circumpapillary circle scan. Each clinical scan consists of 768 A-lines. The circle scan around the optic nerve subtended an angle of 12 degrees. The scan circle diameter in millimeters depends on the axial length, and for a typical eye length, it would measure ~3.5 to 3.6 mm,[28] with some studies suggesting this translating to a 3.45 mm circle.[29–31] A printout was produced from the measurement, including the overall RNFL (360 degrees), each quadrant, and 4 octants or sectors (ST, SN, IT, and IN; Fig. 1).

Analyses of the volume scans were performed using an in-house MATLAB program (MathWorks Inc., Natick, MA). Four annuli were created (Fig. 1): circumpapillary annulus 1 (CA1) was bounded by 2.5 and 3.5 mm diameter circles (Fig. 1, top left), CA2 by 3 and 4 mm circles (Fig. 1, second left), CA3 by 3.5 and 4.5 mm circles (Fig. 1, third left), and CA4 by 4 and 5 mm circles (Fig. 1, bottom left). The MATLAB program automatically centered the circular grids on the ONH (Fig. 1, top right). The MATLAB program segmented the retinal pigmented epithelium/Bruch membrane layer (RPE/BM) in each of the 193 frames and determined the disc region from the termination of the RPE/BM. The disc appears as an elliptical hole when RPE was reconstructed. The center of the ONH was the centroid of the disc.

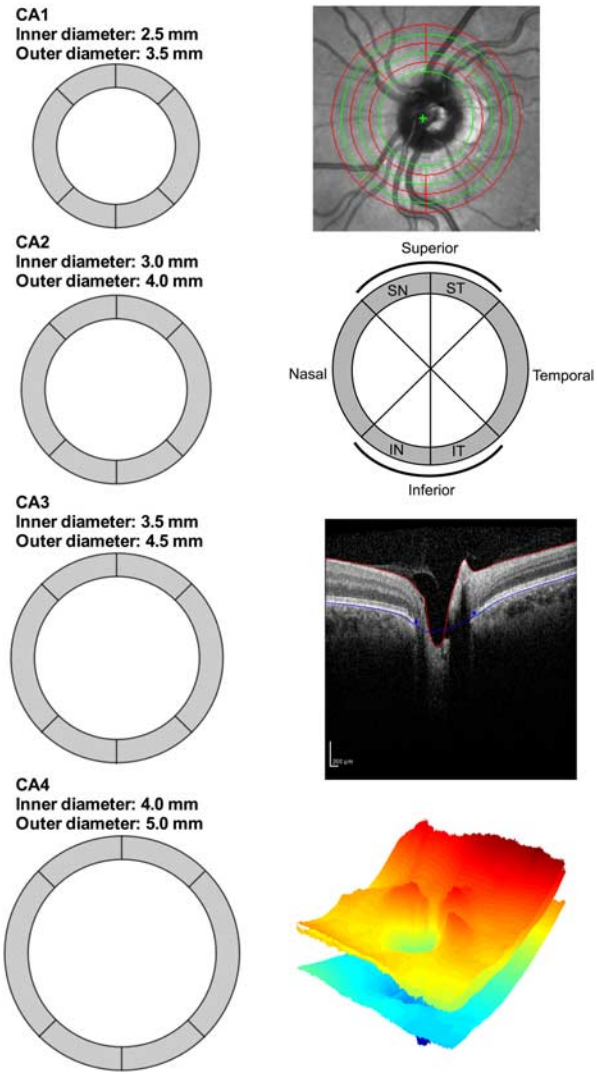


**FIGURE 1.** In-house MATLAB program calculates peripapillary retinal volume measurements from Spectralis volume scans. Left column: a schematic representation and definition of circumpapillary annulus (CA) 1 to 4. Top right: annuli superposed on fundus. Second right: quadrants and sectors/octants in a left eye: superior-temporal (ST), superior-nasal (SN), inferior-temporal (IT), inferior-nasal (IN). Third right: automatic segmentation of the retina. Bottom right: 3D retinal nerve fiber layer and retinal topography.

Despite using a high-density 20×20-degree scan area in volumetric scans, larger annuli sometimes exceeded the scanned regions, and they were excluded by the MATLAB program. Each annulus was divided into four 90-degree quadrants: superior (S), temporal (T), inferior (I), and nasal (N). The superior and inferior quadrants were further divided into 4 octants/sectors: superior-temporal (ST), superior-nasal (SN), inferior-temporal (IT), inferior-nasal (IN) (Fig. 1, second right). The octants and quadrants were defined by drawing geometric horizontal and vertical lines. The software automatically segmented the inner limiting membrane and the RPE/BM complex, by using edge and pixel intensity information in the B-scans and by using the layer definitions outlined in International Nomenclature for OCT Panel[32] (Fig. 1, third right). In each of the 193 B-scans, the inner limiting membrane and RPE/BM complex were constructed as surfaces in 3D to calculate the RV. The tissue volumes that fell between the surfaces were measured by the program for global, quadrant and octant/sector regions in each of the annuli. The investigators performed thousands of RV calculations using the MATLAB software to optimize the segmentation capability before conduction of the study. Multiple calculations of the RV of each study subject were conducted to ensure accuracy. Topography of major retinal layers was shown by color maps (Fig. 1, bottom right). All B-scans were checked for algorithm errors. Artifacts were identified by visual inspection based on methods described previously.[9] Briefly, each B-scan was checked for anterior and posterior segmentation errors, decentration of circular grid over ONH, missing parts, cut edge or truncation. When detected, these were corrected by interpolation of correctly segmented frames. For all 4 annuli sizes, custom-designed software determined mean RV for overall RV (360 degrees), each RV quadrant, and 4 octants (SN, ST, IN, IT; see Fig. 1, second right).

## Statistical Analysis

The demographics of normal versus OAG subjects were compared using $\chi^2$ tests or nonpaired 2-tailed Student *t* tests. Using the clinical diagnosis (OAG vs. normal) as the reference standard, 3D RV and 2D RNFL thickness diagnostic test characteristics (ie, sensitivity, specificity, positive and negative predictive values, and positive and negative likelihood ratios) for all of the quadrants and octants of CA1 to CA4 were calculated using the cutoff value of RV that gave the maximal Youden index (*J*), or [sensitivity +specificity−1). The area under the receiver operating characteristic (AUROC) curves for RV parameters were compared with RNFL thickness parameters for the global, quadrant, and octant regions for all 4 RV annuli sizes and for the 1 RNFL circle size. Differences were considered significant at $P < 0.05$ after FDR correction for multiple testing using the method of Benjamin and Hochberg.[33] FDR-adjustment was performed separately for comparisons between RV values of different annuli, and RV-RNFL comparisons. To quantify the artifact rates, the number of scans with at least one artifact was divided by the total number of B-scans, which, in the case of SD-OCT volume scans, included 193 B-scans for each patient. All statistical analyses were performed using R statistical software version 3.3.2 and the R package AUC version 0.3.0 (Foundation for Statistical Computing, Vienna, Austria). All results are stated as means ± SD unless otherwise stated.

## RESULTS

Of the 180 study subjects, 67 had normal eyes and 113 had OAG. Mean age was 62.7 ± 15.4 years, and 47.8% (86/180) were male. This is a mixed race cohort: 65% (117/180) were white, 18.3% (33/180) were African American, 7.8% (14/180) were Hispanic, 6.1% (11/180) were Asian, and 2.8% (5/180) were other race. OAG patients were older than normal subjects by 13.9 years ($P < 0.0001$) and had worse VF performance ($P < 0.0001$, Table 1).

A larger annular size was associated with a higher percentage of regions outside the 20×20-degree scan area. Specifically, zero of 180 scans from CA1, 3 scans (1.7%) from CA2, 10 scans (5.5%) from CA3, and 13 scans (7.2%) from CA4 were excluded.

**TABLE 1.** Demographics of the Normal and Open-angle Glaucoma Study Population

| | Normal | OAG | P* |
|---|---|---|---|
| No. eyes | 67 | 113 | |
| No. right eyes/left eyes | 31/36 | 63/50 | 0.28 |
| Sex (male/female) | 20/47 | 66/47 | 0.0002 |
| Mean age ± SD (y) | 54.0 ± 16.5 | 67.9 ± 12.1 | < 0.0001 |
| Refractive error (D) | | | |
| Spherical equivalent ± SD | −0.46 ± 1.86 | −0.67 ± 1.84 | 0.49 |
| Visual field (dB) | | | |
| Mean deviation | −1.40 ± 1.90 | −12.5 ± 7.73 | < 0.0001 |
| Pattern standard deviation | 1.50 ± 0.28 | 8.51 ± 3.41 | < 0.0001 |

*$P$-values obtained from $\chi^2$ tests for categorical valuables and 2-tailed Student $t$ tests for continuous variables.

OAG indicates open-angle glaucoma.

OAG patients had lower RV values compared with normal patients for global, quadrants, and octants across all 4 annuli sizes ($P < 0.0001$ for all, Table 2). AUROC values for RV for all annuli sizes, quadrants, and octants were consistently above 0.8 (Table 3). Inferior quadrant RV demonstrated the highest AUROC curve values (0.964) compared with global RV and other individual quadrant or octant RV values in their respective annuli (Table 3). The highest AUROC values were those associated with inferior RV of CA1 and CA2 (0.964 and 0.955, respectively, Table 3) and with inferior, IT, and global RNFL thickness (0.966, 0.965, and 0.959, respectively, Table 3). Supplementary Figures 1 to 3 (Supplemental Digital Content 1, http://links.lww.com/IJG/A269) provide a graphic representation of AUROC values, sensitivities, and specificities for inferior and global RV of CA1, as well as global RNFL thickness.

Table 4 shows the sensitivities and specificities for RV of CA1 and RNFL at the cutoff values that maximize the Youden index. The best sensitivities were those associated with IT octant of RNFL, inferior RV of CA4, inferior RV of CA1, inferior quadrant of RNFL, and IT RV of CA4 (0.946, 0.946, 0.938, 0.911, 0.901, respectively). The best specificities were those associated with global RNFL, inferior RNFL, temporal RV of CA4, global RV of CA3 (0.970, 0.970, 0.955, 0.952, respectively).

Looking more closely at the regions with the highest AUROC curves, a cutoff value of 90.5 μm for inferior quadrant of RNFL thickness correctly predicted 102 of 112 OAG cases (91.1% sensitivity) (1 case was missing RNFL thickness value for the inferior quadrant), and a normal diagnosis in 65 out of 67 cases (97.0% specificity, Table 4). A cutoff value of 0.38063 $mm^3$ for CA1's inferior RV correctly predicted OAG in 106 of 113 cases (93.8% sensitivity), and a normal diagnosis in 62 of 67 cases (92.5% specificity, Table 4, Supplementary Fig. 1, Supplemental Digital Content 1, http://links.lww.com/IJG/A269).

In Table 5, global AUROC for all the annuli were not statistically different from each other among all the pair-wise comparisons ($P > 0.05$ for all). Similarly, in inferior and superior quadrant analyses, none of the RV annuli were significantly different from each other in pair-wise comparisons ($P > 0.05$ for all). On the other hand, in octant analyses, the annuli closer to the optic disc (ie, CA1, CA2) consistently had better diagnostic performance in IT and IN octants compared with annuli farther away from the optic disc (ie, CA3 and CA4, Table 5). For example, CA1 had a higher AUROC value in the IT octant compared with CA2, CA3, CA4 ($P = 0.037$ for all), and in the IN octant compared with CA2, CA3, CA4 ($P = 0.037$, 0.037, 0.0038, respectively). Similar patterns were observed when comparing inferior octants of CA2 with those of CA3, CA4, although not all were statistically significant (Table 5). In addition, ST octant of CA4 consistently had lower AUROC values compared with CA1, CA2, and CA3 ($P = 0.037$, 0.0163, 0.037, respectively). On the other hand, AUROC of the SN octant of all 4 annuli were not significantly different when compared pair-wise ($P > 0.05$). In temporal and nasal quadrant analyses, there was no significant difference in the temporal or nasal quadrants of all 4 annuli in pair-wise comparisons ($P > 0.05$ for all).

**TABLE 2.** Mean Retinal Volume and Retinal Nerve Fiber Layer Thickness Measurements for Normal and Open-angle Glaucoma Patients

| | Global | Superior | Temporal | Inferior | Nasal | Superior-temporal | Superior-nasal | Inferior-temporal | Inferior-nasal |
|---|---|---|---|---|---|---|---|---|---|
| Retinal volume—4 circumpapillary (CA) annuli sizes | | | | | | | | | |
| CA1 ($mm^3$)* | | | | | | | | | |
| Normal | 1.58 | 0.42 | 0.38 | 0.42 | 0.36 | 0.21 | 0.21 | 0.21 | 0.21 |
| OAG | 1.34 | 0.35 | 0.34 | 0.33 | 0.32 | 0.18 | 0.17 | 0.17 | 0.17 |
| CA2 ($mm^3$)* | | | | | | | | | |
| Normal | 1.76 | 0.46 | 0.44 | 0.46 | 0.40 | 0.23 | 0.23 | 0.23 | 0.23 |
| OAG | 1.52 | 0.39 | 0.39 | 0.37 | 0.36 | 0.20 | 0.19 | 0.19 | 0.19 |
| CA3 ($mm^3$)* | | | | | | | | | |
| Normal | 1.94 | 0.50 | 0.50 | 0.50 | 0.44 | 0.25 | 0.25 | 0.25 | 0.25 |
| OAG | 1.70 | 0.43 | 0.45 | 0.41 | 0.41 | 0.22 | 0.21 | 0.21 | 0.21 |
| CA4 ($mm^3$)* | | | | | | | | | |
| Normal | 2.12 | 0.54 | 0.56 | 0.54 | 0.48 | 0.27 | 0.27 | 0.27 | 0.27 |
| OAG | 1.88 | 0.47 | 0.51 | 0.45 | 0.44 | 0.24 | 0.23 | 0.23 | 0.23 |
| RNFL thickness—1 circle scan size | | | | | | | | | |
| RNFL (μm)* | | | | | | | | | |
| Normal | 93.8 | 113 | 69.5 | 122 | 70.5 | 127 | 98.6 | 137 | 107 |
| OAG | 58.0 | 69.2 | 50.0 | 63.0 | 49.5 | 75.0 | 63.3 | 63.5 | 62.6 |

*$P < 0.0001$ for all values, when comparing normal versus OAG groups using 2-tailed Student $t$ tests for continuous variables.

CA1 indicates smallest circumpapillary annulus bounded by circular grids with diameters of 2.5 and 3.5 mm; CA2, circumpapillary annulus bounded by diameters of 3 and 4 mm; CA3, circumpapillary annulus bounded by diameters of 3.5 and 4.5 mm; CA4, largest circumpapillary annulus bounded by diameters of 4 and 5 mm; OAG, open-angle glaucoma; RNFL, retinal nerve fiber layer.

**TABLE 3.** Area Under the Receiver Operating Characteristic Curve of Peripapillary Retinal Volume and Retinal Nerve Fiber Layer Thickness for Normal Versus Primary Open-angle Glaucoma Patients

| | AUROC (SE) | | | | |
|---|---|---|---|---|---|
| | RV | | | | RNFL Thickness |
| | CA1 (2.5-3.5 mm) | CA2 (3-4 mm) | CA3 (3.5-4.5 mm) | CA4 (4-5 mm) | RNFL (3.45 mm) |
| Global | 0.937 (0.017) | 0.929 (0.019) | 0.929 (0.020) | 0.912 (0.023) | 0.959 (0.013) |
| Superior | 0.928 (0.019) | 0.934 (0.017) | 0.934 (0.017) | 0.915 (0.021) | 0.937 (0.017) |
| Temporal | 0.834 (0.029) | 0.830 (0.030) | 0.823 (0.030) | 0.816 (0.032) | 0.854 (0.029) |
| Inferior | 0.964 (0.013) | 0.955 (0.015) | 0.945 (0.018) | 0.945 (0.018) | 0.966 (0.012) |
| Nasal | 0.837 (0.030) | 0.831 (0.031) | 0.823 (0.032) | 0.817 (0.034) | 0.829 (0.031) |
| ST | 0.917 (0.020) | 0.908 (0.022) | 0.900 (0.023) | 0.874 (0.026) | 0.933 (0.019) |
| SN | 0.904 (0.023) | 0.899 (0.023) | 0.889 (0.024) | 0.863 (0.030) | 0.869 (0.026) |
| IT | 0.947 (0.017) | 0.931 (0.019) | 0.919 (0.021) | 0.910 (0.022) | 0.965 (0.013) |
| IN | 0.950 (0.015) | 0.927 (0.020) | 0.904 (0.025) | 0.877 (0.028) | 0.905 (0.021) |

AUROC indicates area under receiving receiver operating characteristic curve; CA1, smallest circumpapillary annulus bounded by circular grids with diameters of 2.5 and 3.5 mm; CA2, circumpapillary annulus bounded by diameters of 3 and 4 mm; CA3, circumpapillary annulus bounded by diameters of 3.5 and 4.5 mm; CA4, circumpapillary annulus by diameters of 4 and 5 mm; IN, inferior-nasal; IT, inferior-temporal; RNFL, retinal nerve fiber layer; SN, superior-nasal; ST, superior-temporal.

In pair-wise comparisons between RNFL thickness and RV measurements (Table 5), RNFL thickness and RV had similar diagnostic capability among all quadrants and octants, and across all 4 annuli ($P > 0.05$).

In addition, even though OAG patients were significantly older than normal subjects (Table 1), AUROC values with and without age adjustment were not significantly different from each other ($P > 0.05$ for all, Supplementary Table 1, Supplemental Digital Content 2, http://links.lww.com/IJG/A270).

Among all patients' RV scans or 34,740 B-scans (193 B-scans per 180 eyes), a total of 2071 scans (6.0%) had at least 1 artifact (Table 6). Among them, 2.5% (852/34,740) were anterior segmentation errors, and 1.5% (521/34,740) were posterior (RPE/BM) segmentation errors. No decentration errors were identified. In contrast, in the same set of 180 patients, 2D RNFL scans had an overall artifact rate of 32.2% (58/180). Among them, 5.6% (10/180) were anterior segmentation errors, and 22.2% (40/180) were posterior (RNFL layer) segmentation errors, and 9.4% (17/180) were decentration artifacts. No cut edge or mirror artifacts were seen among this set of RNFL scans. When comparing RV versus RNFL thickness, RV had a significantly lower artifact rate per B-scan compared with RNFL scans ($P < 0.0001$, Table 6). RV also had significantly lower artifact rates in the 3 individual artifact rate categories that were compared, including anterior segmentation error, posterior segmentation error, and missing part artifact ($P < 0.0001$ for all, Table 6). In addition, artifact rates for RV and RNFL thickness were also analyzed separately for normal participants and glaucoma patients. The results were very similar to when the groups were analyzed together: RV had significantly lower artifact rates among both normal participants and glaucoma patients.

## DISCUSSION

In this study, we compared the traditional commercially available 2D peripapillary RNFL thickness parameter with fixed scan circle sizes to a new 3D peripapillary RV parameter, which can be calculated using novel software which was specifically designed for glaucoma diagnosis and which allows for customizable scan circle sizes. There is a need for commercially available glaucoma software customized for high-density analysis of the peripapillary retina, because current commercially available software primarily allows for high-density analysis of the peripapillary retina[20,22] by moving the ETDRS fixed-sized scan circles, which were designed for analysis of diabetic macular disease, over the optic nerve instead of the fovea. For this paper, peripapillary RVs were obtained from 3D volume scans using new customized software, with different adjustable annuli sizes (CA1 with 2.5 and 3.5 mm diameters; CA2 with 3 and 4 mm diameters; CA3 with 3.5 and 4.5 mm diameters; CA4 with 4 and 5 mm diameters). We also determined that the best circumpapillary RV annulus sizes for glaucoma diagnosis was the smallest annuli CA1 (2.5 to 3.5 mm). For diagnosing perimetric OAG, this CA1 annulus was equal to that of the traditional 2D RNFL thickness parameters, and better than that of CA2, CA3, and CA4, especially in the inferior octants. When determining which region had the best diagnostic ability, the inferior quadrant RV consistently showed the best diagnostic capability compared with both other quadrants as well as global RV and octant RV regions for all annuli sizes. The segmentation artifact rates for RV (ie, 6% of B-scans) were also lower than that reported in this study (32.2% of RNFL scans, $P < 0.0001$, Table 6) and in the literature for RNFL thickness at 19.9% to 46.3%.[8,9]

Even though peripapillary RNFL thickness is the most commonly studied glaucoma OCT parameter, there is evidence to suggest that glaucomatous arcuate defects were sometimes more easily identified in peripapillary RT maps.[34] When focusing on the peripapillary region for glaucomatous disease, this pilot data further implied that quantitative analysis of the peripapillary region does not need to be limited to just RNFL thickness but can also include RT and RV. Because of this pilot data,[34] larger studies were then conducted to further test this concept and to evaluate peripapillary RT and RV as new clinical parameters for clinical glaucoma care.[20,22] These larger studies of normal and glaucoma patients showed that peripapillary RT and 3D peripapillary RV may have the same or better diagnostic ability as traditional 2D peripapillary RNFL thickness, largely due to having fewer segmentation artifacts.[20,22] Before these studies, total RT measurements

 

**TABLE 4.** Diagnostic Ability of Best 3D Circumpapillary Retinal Volume Annulus Versus 2D Retinal Nerve Fiber Layer Thickness in Diagnosing Open-angle Glaucoma

| | Cutoff Value ($mm^3$ or μm) | Sensitivity (95% CI) | Specificity (95% CI) | PPV (95% CI) | NPV (95% CI) | PLR (95% CI) | NLR (95% CI) |
|---|---|---|---|---|---|---|---|
| 3D Peripapillary retinal volume ($mm^3$) for CA1 (inner diameter 2.5 mm, outer diameter 3.5 mm)* | | | | | | | |
| Global | 1.445 | 0.858 (0.780-0.917) | 0.940 (0.854-0.984) | 0.960 (0.902-0.989) | 0.798 (0.692-0.880) | 14.4 (5.54-37.3) | 0.151 (0.095-0.238) |
| Superior | 0.387 | 0.858 (0.780-0.917) | 0.910 (0.815-0.966) | 0.942 (0.878-0.978) | 0.792 (0.685-0.876) | 9.59 (4.45-20.6) | 0.156 (0.098-0.246) |
| Temporal | 0.347 | 0.664 (0.569-0.750) | 0.925 (0.834-0.975) | 0.938 (0.860-0.979) | 0.620 (0.518-0.715) | 8.89 (3.79-20.9) | 0.363 (0.278-0.475) |
| Inferior | 0.381 | 0.938 (0.877-0.975) | 0.925 (0.834-0.975) | 0.955 (0.898-0.985) | 0.899 (0.802-0.958) | 12.6 (5.40-29.2) | 0.067 (0.033-0.138) |
| Nasal | 0.342 | 0.805 (0.720-0.874) | 0.791 (0.674-0.881) | 0.867 (0.786-0.925) | 0.707 (0.590-0.806) | 3.85 (2.40-6.20) | 0.246 (0.166-0.365) |
| ST | 0.192 | 0.814 (0.730-0.881) | 0.910 (0.815-0.966) | 0.939 (0.872-0.977) | 0.744 (0.636-0.834) | 9.09 (4.22-19.6) | 0.204 (0.138-0.302) |
| SN | 0.195 | 0.867 (0.791-0.924) | 0.806 (0.691-0.892) | 0.883 (0.808-0.936) | 0.783 (0.667-0.873) | 4.47 (2.73-7.32) | 0.165 (0.101-0.268) |
| IT | 0.189 | 0.885 (0.811-0.937) | 0.910 (0.815-0.966) | 0.943 (0.881-0.979) | 0.824 (0.718-0.903) | 9.88 (4.59-21.3) | 0.126 (0.075-0.212) |
| IN | 0.187 | 0.867 (0.791-0.924) | 0.925 (0.834-0.975) | 0.952 (0.890-0.984) | 0.805 (0.699-0.887) | 11.6 (4.99-27.1) | 0.143 (0.089-0.231) |
| 2D Peripapillary RNFL thickness (μm) | | | | | | | |
| Global | 72.0 | 0.821 (0.738-0.887) | 0.970 (0.896-0.996) | 0.979 (0.925-0.997) | 0.765 (0.660-0.850) | 27.5 (7.01-108) | 0.184 (0.124-0.274) |
| Superior | 88.0 | 0.813 (0.728-0.880) | 0.925 (0.834-0.975) | 0.948 (0.883-0.983) | 0.747 (0.640-0.836) | 10.9 (4.66-25.4) | 0.203 (0.137-0.300) |
| Temporal | 57.5 | 0.759 (0.669-0.835) | 0.881 (0.778-0.947) | 0.914 (0.838-0.962) | 0.686 (0.577-0.782) | 6.36 (3.29-12.3) | 0.274 (0.195-0.385) |
| Inferior | 90.5 | 0.911 (0.842-0.956) | 0.970 (0.896-0.996) | 0.981 (0.932-0.998) | 0.867 (0.768-0.934) | 30.5 (7.78-120) | 0.092 (0.051-0.167) |
| Nasal | 67.5 | 0.866 (0.789-0.923) | 0.657 (0.531-0.769) | 0.808 (0.726-0.874) | 0.746 (0.616-0.850) | 2.53 (1.80-3.54) | 0.204 (0.124-0.337) |
| ST | 108.5 | 0.893 (0.820-0.943) | 0.866 (0.760-0.937) | 0.917 (0.849-0.962) | 0.829 (0.720-0.908) | 6.65 (3.61-12.2) | 0.124 (0.072-0.213) |
| SN | 69.5 | 0.652 (0.556-0.739) | 0.925 (0.834-0.975) | 0.936 (0.857-0.979) | 0.614 (0.512-0.709) | 8.73 (3.72-20.5) | 0.376 (0.290-0.489) |
| IT | 109 | 0.946 (0.887-0.980) | 0.925 (0.834-0.975) | 0.955 (0.898-0.985) | 0.912 (0.818-0.967) | 12.7 (5.45-29.5) | 0.058 (0.027-0.127) |
| IN | 75.5 | 0.741 (0.650-0.819) | 0.910 (0.815-0.966) | 0.933 (0.859-0.975) | 0.678 (0.571-0.773) | 8.28 (3.83-17.9) | 0.284 (0.206-0.393) |

2D indicates 2-dimensional; 3D, 3-dimensional; CA1, smallest circumpapillary annulus bounded by circular grids with diameters of 2.5 and 3.5 mm; CI, confidence interval; IN, inferior-nasal; IT, inferior-temporal; NLR, negative likelihood ratio; NPV, negative predictive value; OAG, open-angle glaucoma; PLR, positive likelihood ratio; PPV, positive predictive value; RNFL, retinal nerve fiber layer; SN, superior-nasal; ST, superior-temporal.

*Although 4 annuli sizes were evaluated in this study (ie, CA1 to CA4), Table 4 only presents the results of the smallest annulus CA1, which had the best diagnostic ability for glaucoma.

**TABLE 5.** Pair-wise Comparisons of the Diagnostic Abilities for Retinal Volume and Retinal Nerve Fiber Layer Thickness

| | Global | Superior | Temporal | Inferior | Nasal | ST | SN | IT | IN |
|---|---|---|---|---|---|---|---|---|---|
| CA1 vs. CA2 | | | | | | | | | |
| ΔAUROC* | 0.0076 | −0.0054 | 0.0042 | 0.0087 | 0.0056 | 0.0086 | 0.0052 | 0.0163 | 0.0237 |
| *P*† | 0.082 | 0.444 | 0.584 | 0.081 | 0.208 | 0.444 | 0.569 | 0.037 | 0.037 |
| CA1 vs. CA3 | | | | | | | | | |
| ΔAUROC | 0.0077 | −0.0059 | 0.0107 | 0.0183 | 0.0131 | 0.0203 | 0.0149 | 0.0278 | 0.0461 |
| *P* | 0.173 | 0.630 | 0.527 | 0.082 | 0.081 | 0.082 | 0.322 | 0.037 | 0.037 |
| CA1 vs. CA4 | | | | | | | | | |
| ΔAUROC | 0.0245 | 0.0133 | 0.0180 | 0.0182 | 0.0196 | 0.0421 | 0.0411 | 0.0370 | 0.0735 |
| *P* | 0.076 | 0.509 | 0.545 | 0.081 | 0.082 | 0.037 | 0.115 | 0.037 | 0.0038 |
| CA2 vs. CA3 | | | | | | | | | |
| ΔAUROC | 0.0001 | −0.0005 | 0.0065 | 0.0096 | 0.0075 | 0.0117 | 0.0097 | 0.0115 | 0.0224 |
| *P* | 0.719 | 0.975 | 0.545 | 0.113 | 0.081 | 0.049 | 0.163 | 0.113 | 0.037 |
| CA2 vs. CA4 | | | | | | | | | |
| ΔAUROC | 0.0169 | 0.0187 | 0.0138 | 0.0095 | 0.0140 | 0.0335 | 0.0359 | 0.0207 | 0.0498 |
| *P* | 0.116 | 0.159 | 0.577 | 0.082 | 0.106 | 0.0163 | 0.076 | 0.061 | 0.0016 |
| CA3 vs. CA4 | | | | | | | | | |
| ΔAUROC | 0.0168 | 0.0192 | 0.0073 | −0.0001 | 0.0065 | 0.0218 | 0.0262 | 0.0092 | 0.0274 |
| *P* | 0.081 | 0.113 | 0.642 | 0.741 | 0.235 | 0.037 | 0.081 | 0.037 | 0.0039 |
| RNFL vs. CA1 | | | | | | | | | |
| ΔAUROC | 0.0229 | 0.0081 | 0.0205 | 0.0024 | −0.0071 | 0.0165 | −0.0345 | 0.0173 | −0.0452 |
| *P* | 0.270 | 0.738 | 0.652 | 0.911 | 0.911 | 0.610 | 0.447 | 0.452 | 0.139 |
| RNFL vs. CA2 | | | | | | | | | |
| ΔAUROC | 0.0305 | 0.0027 | 0.0247 | 0.0111 | −0.0015 | 0.0251 | −0.0293 | 0.0336 | −0.0215 |
| *P* | 0.181 | 0.911 | 0.610 | 0.570 | 0.911 | 0.452 | 0.452 | 0.199 | 0.570 |
| RNFL vs. CA3 | | | | | | | | | |
| ΔAUROC | 0.0306 | 0.0022 | 0.0312 | 0.0209 | 0.0060 | 0.0368 | −0.0196 | 0.0451 | 0.0009 |
| *P* | 0.181 | 0.911 | 0.570 | 0.447 | 0.911 | 0.322 | 0.652 | 0.139 | 0.956 |
| RNFL vs. CA4 | | | | | | | | | |
| ΔAUROC | 0.0474 | 0.0214 | 0.0385 | 0.0206 | 0.0125 | 0.0586 | 0.0066 | 0.0543 | 0.0283 |
| *P* | 0.139 | 0.610 | 0.510 | 0.447 | 0.652 | 0.199 | 0.911 | 0.139 | 0.570 |

*ΔAUROC, or difference in AUROC, is calculated by subtracting the AUROC of retinal volume of the second annulus from that of the first annulus (ie, ΔAUROC of CA1 vs. CA2 represents AUROC of CA1 minus CA2).

†All *P*-values were obtained from pair-wise comparisons, correspond to *P*-values after FDR correction for multiple testing using the method of Benjamini and Hochberg.[33] FDR-adjustment was performed separately for comparisons between RV values of different annuli, and RV-RNFL comparisons.

AUROC indicates area under the receiver operating characteristic curve; CA1, inner circumpapillary annulus bounded by circular grids with diameters of 2.5 and 3.5 mm; CA2, circumpapillary annulus bounded by diameters of 3 mm and 4 mm; CA3, circumpapillary annulus 3 bounded diameters of 3.5 and 4.5 mm; CA4, circumpapillary annulus by diameters of 4 and 5 mm; IN, inferior-nasal; IT, inferior-temporal; RNFL, retinal nerve fiber layer; SN, superior-nasal; ST, superior-temporal.

were primarily used for the evaluation of retinal diseases of the macula, such as the use of ETDRS circles for diabetic retinopathy, and not for peripapillary analysis of the retina for glaucomatous disease. In addition, the use of RT and RV maps for glaucoma evaluation makes theoretical sense, because the top-most retinal layers, both RNFL and ganglion cell layer, are affected by glaucoma on histology. Lastly, current commercially available glaucoma software which calculates macular parameters may be limited by nonglaucomatous macular pathology such as macular degeneration or diabetes, so maximizing use of all available regions of interest, including the peripapillary region, would help to provide best comprehensive analysis of the entire posterior pole in glaucoma.

**TABLE 6.** Artifact Rate Comparison Between 3D Retinal Volume Scans and 2D Retinal Nerve Fiber Layer Thickness Scans Among All Subjects

**Artifact Rates and Comparison among All Subjects**

| Artifact Type | RV (All) [N (%)] | RNFL (All) [N (%)] | *P** |
|---|---|---|---|
| Overall | 2071 (6.0) | 58 (32.2) | < 0.0001 |
| Anterior segmentation | 852 (2.5) | 10 (5.6) | < 0.0001 |
| Posterior segmentation | 521 (1.5) | 40 (22.2) | < 0.0001 |
| Decentration | 0 | 17 (9.4) | NA |
| Missing parts | 153 (0.4) | 7 (3.9) | < 0.0001 |
| Cut edge | 651 (1.9) | 0 | NA |
| Mirror artifact | 28 (0.08) | 0 | NA |

*All *P*-values were obtained from comparisons using Fisher exact test to compare artifact rates between retinal volume measurements versus retinal nerve fiber layer.

NA indicates not available; OAG, open-angle glaucoma; RNFL, retinal nerve fiber layer; RV, retinal volume.

In this study, we found that RV in the CA1 region was the best parameter for glaucoma because areas beyond the 2.5 to 3.5 mm annular region likely comprised of retina with a proportionately smaller amount of RNFL (Tables 3, 5). Therefore, our MATLAB software program was able to confirm that the 2.5 to 3.5 mm peripapillary region is most sensitive for detecting glaucomatous disease and that the ETDRS circles are larger and may be more suitable for evaluating diabetic or macular disease. Specifically, in our investigation, we chose annuli with inner diameters from 2.5 mm to outer diameters of 5 mm with 0.5 mm increments, in order to quantify peripapillary retinal tissue volume. Previously, our group investigated the diagnostic capability of peripapillary RT and RV measurements, which were obtained by centering the ETDRS circular grid around the

ONH instead of over the fovea.[20,22] Even though the ETDRS grids were designed to evaluate the macular region in patients with diabetic retinopathy, we used the ETDRS circular grid and its set dimensions (diameters of 1, 2, 3 mm; 1, 2.22, 3.45 mm; and 1, 3, 6 mm) since it was already built into the Heidelberg system for macular imaging. When using these ETDRS grids over the ONH instead of the macula, we found that peripapillary RT and RV measurements still had excellent diagnostic capability, comparable to, if not better than, that of RNFL thickness measurements in glaucoma.[17,18] As a result of these promising data, our group developed customized software to measure peripapillary RV using a new set of circumpapillary annuli, whose inner and outer diameters could be varied to any diameter. While selecting for the appropriate annular sizes, we took into account data from our previous studies that (1) RT and RV measurements from annuli of smaller diameter, such as those bounded by ETDRS diameter circles of 2 and 3 mm, had better diagnostic accuracy compared with measurements from larger annuli, such as those bounded by ETDRS diameter circles of 3 and 6 mm, (2) the annulus bounded by diameters of 2, 3 mm and 2.22 and 3.45 mm were least affected by peripapillary atrophy (PPA), (3) as much as 23.7% of the scans fell out of the 6×6 mm scanned region for the largest annulus bounded by diameters 3 and 6 mm.[17] Indeed, only 7.2% of the annuli fell outside of the 6 mm×6 mm scanned area for our largest annuli CA4, bounded by circles of diameters 4 and 5 mm.

The annulus with the highest global RV diagnostic performance was that closest to the ONH, namely CA1 (global CA1 AUOC 0.937, Tables 3, 4), even though *P*-values were borderline at 0.082 and 0.076, compared with CA2 and CA4, respectively. This is consistent with the observation that the closer one is to the disc margin, the higher the proportion of RNFL to total RV. An RV annulus closer to the optic nerve, therefore, is more sensitive to glaucomatous changes in the RNFL. In addition, total RV decreases with increased distance from the ONH, so measuring RV at a place where it is thicker allows a higher sensitivity to subtle RV changes compared with where it is thinner with an annulus farther away from the optic disc, such as CA4.[35] However, the annulus should not be too close to the disc border since measurements may be theoretically compromised by pathologies such as PPA. Our previous RT study showed that PPA did not affect the diagnostic capability of RT when using a 2 and 3 mm diameter annulus,[20] and our past RV study showed that PPA did not affect RV's diagnostic capability when using a 2.22 and 3.45 mm diameter annulus around the ONH.[22] The 4 annuli used in this study were all farther away than the ones studied previously, so theoretically the diagnostic performance of the 4 annuli in this study should not be affected by PPA either.

The sensitivity and specificity pattern of the best quadrants and octants for RV diagnostic performance is consistent with our understanding of glaucomatous optic disc change over time and prior observations in RNFL thickness measurements, which suggest that glaucoma preferentially affects the superior and inferior regions (Tables 3, 4). The best diagnostic ability for distinguishing normal from glaucoma patients was for the inferior, superior, IT, and global regions of RV, with the inferior quadrant being consistently better than the superior quadrant (Table 4). This is consistent with the observation that in glaucoma while thinning of the neuroretinal rim occurs in all sectors of the optic disc, there is a preference for the inferior pole that tends to be affected the most and before other regions.[36–39] This is also consistent with the pattern observed previously in RNFL studies, specifically that the inferior and superior quadrants of RNFL thickness conferred the best diagnostic performance in detection of glaucoma using OCT, with added preference for the inferior temporal and superior temporal sectors.[6,26–28,40] This consistency is reassuring in that the anatomical patterns of change, which are captured in RNFL thickness measurements between glaucoma versus normal patients, are also detected in RV measurements (Table 2).

Table 4 also showed that global and temporal quadrants were the most specific, or had the fewest false positives, compared with other regions of RNFL and RV. This is again consistent with known glaucomatous progression that the thinning of inferior and superior RNFL tends to precede that of nasal or temporal RNFL thinning.[39] In addition, the excellent specificities in the nasal and temporal quadrants in this study may also be owing to the fact that 3D volume scans have good sampling of these regions.[41] Recently, several studies that assessed 3D volume parameters demonstrated superior diagnostic capability in the nasal and temporal regions compared with traditional RNFL thickness measurements.[42,43] In addition to temporal region papillomacular bundle sparing in late glaucomatous disease, the temporal optic nerve, and peripapillary region may be less affected by blood vessel imaging artifacts.

One study, using a 3.46 mm-diameter circle scan, showed that inferior RNFL defects tend to be narrower than superior defects among OAG patients with VF defects.[44] It was thought that the increased concentration of RNFL tissue inferiorly was related to the less supportive nature of the lamina cribrosa in the same area with larger single pore sizes.[39,45,46] Our results were consistent with their findings albeit measured in RV: CA1, which is the only annulus in our study that fell completely within the 3.46 diameter circle, was better at capturing the entirety of the narrower, more concentrated inferior defects that fell within a small area. In addition, the narrower inferior defects were better captured in smaller octants compared with a wider quadrant area, thus reaching statistical significance in octant analyses but not quadrant analyses.

The OAG patients in our study were significantly older than normal subjects. This is consistent with the fact that glaucoma incidence increases with age[47–49] and is reflective of the patient population clinicians encounter every day. In order to account for this statistically significant difference, we conducted calculations to adjust for age in AUROC calculations and found that there was not any statistically significant difference between AUROC values with or without age adjustment (Supplementary Table 1, Supplemental Digital Content 2, http://links.lww.com/IJG/A270). Future studies on the normal age-related loss for 3D parameters need to be done.

Our study showed that RV scans had significantly fewer artifacts compared with 2D RNFL scans in the same patient population (6.0% vs. 32.2%, $P < 0.0001$, Table 6), most likely owing to a combination of how our MATLAB software was engineered to minimize artifacts and intrinsic RV characteristics themselves. Our software automatically eliminated one of the most common types of RNFL thickness artifacts, the decentration artifact, which occurred in 9.4% of 2D RNFL scans in this study (Table 6) and in as much as 27.8% of RNFL thickness scans in a large study of

 

over 2000 2D RNFL scans.[9] In addition, RV measurements had significantly fewer algorithm segmentation errors compared with RNFL thickness scans (Table 6). Most notably, while posterior segmentation errors were present in 22.2% of RNFL scans, which was the most common type of 2D RNFL artifact in this study, only 1.5% of B-scans in the volume studies had posterior segmentation errors ($P < 0.0001$, Table 6). This major difference is most likely related to the loss of RNFL reflectivity in glaucomatous eyes, making it difficult for algorithms to distinguish the posterior RNFL border from the underlying structures.[18] On the other hand, there is no evidence in the literature to suggest that glaucoma causes a loss of reflectivity in the RPE/BM complex, which is the posterior border of RV. Indeed, the difference between posterior segmentation errors of RNFL thickness versus RV was most prominent among OAG patients (27.4% vs. 1.2%, $P < 0.0001$, Table 6). Other possible factors that account for this difference include better computer software and better scan quality with volume scans, which would also significantly decrease posterior segmentation artifacts among normal patients (13.4% vs. 1.6%, $P < 0.0001$, Table 6).

Lower artifact rates in OCT imaging is clinically significant as OCT artifacts are known to cause clinically significant measurement errors.[50] Recently, Mansberger and associates showed that automated segmentation by OCT without manual refinement led to lower global RNFL thickness values and over-classification of glaucoma.[51] As much as 23.7% of borderline classifications, or yellow coding on OCT, became normal after manual refinement of segmentation. This "yellow disease," along with red disease (false positives) and green disease (false negatives), can be minimized by better imaging scan protocols, such as with OCT volume scans; algorithm refinement, such as with automated centration; better segmentation algorithms, such as those customized for glaucoma; and better diagnostic parameters, such as RV.

Our study has several limitations. Our study is limited by spectrum bias,[52] or the fact that all our OAG patients had reliable VF defects with a mean MD of $<-12$ dB. Therefore, our findings are not generalizable to all glaucoma patients, and our diagnostic accuracy can be biased or overestimated. As structural defects are known to precede functional VF loss, future studies that aim to study the diagnostic value of RV in preperimetric glaucoma would be valuable. In addition, unlike clinical OCT examinations where the cutoff values are based on a normative database of a large number of diverse patient population, our cutoff values were selected to maximize the Youden index and the diagnostic capability in this specific set of 180 patients. The cutoff values of our study, therefore, may not be broadly generalizable. Also, the AUROC curve values of our study may not be applicable to a larger patient population or when cutoff values are obtained from a normative database.

Nonetheless, our study showed that 3D peripapillary RV has similar diagnostic capability for OAG compared with the widely used 2D RNFL thickness measurement. RV measurements had lower artifact rates compared with RNFL thickness scans (6.0% vs. 32.2%, $P < 0.0001$, Table 6), making it a more reliable imaging parameter for diagnostic purposes. Best RV regions and annuli sizes included the inferior quadrant and the CA1 annulus, bounded by circular diameters of 2.5 and 3.5 mm. However, future studies are needed to better assess the clinical utility of 2D versus 3D glaucoma SD-OCT parameters.

## REFERENCES


1. Tham Y-C, Li X, Wong TY, et al. Global prevalence of glaucoma and projections of glaucoma burden through 2040: a systematic review and meta-analysis. *Ophthalmology*. 2014;121:2081–2090.
2. Kingman S. Glaucoma is second leading cause of blindness globally. *Bull World Health Organ*. 2004;82:887–888.
3. Maier PC, Funk J, Schwarzer G, et al. Treatment of ocular hypertension and open angle glaucoma: meta-analysis of randomised controlled trials. *BMJ*. 2005;331:134.
4. Wu H, de Boer JF, Chen TC. Diagnostic capability of spectral-domain optical coherence tomography for glaucoma. *Am J Ophthalmol*. 2012;153:815–826.e2.
5. Sung KR, Na JH, Lee Y. Glaucoma diagnostic capabilities of optic nerve head parameters as determined by Cirrus HD optical coherence tomography. *J Glaucoma*. 2012;21:498–504.
6. Schulze A, Lamparter J, Pfeiffer N, et al. Diagnostic ability of retinal ganglion cell complex, retinal nerve fiber layer, and optic nerve head measurements by Fourier-domain optical coherence tomography. *Graefes Arch Clin Exp Ophthalmol*. 2011;249:1039–1045.
7. Na JH, Sung KR, Lee JR, et al. Detection of glaucomatous progression by spectral-domain optical coherence tomography. *Ophthalmology*. 2013;120:1388–1395.
8. Asrani S, Essaid L, Alder BD, et al. Artifacts in spectral-domain optical coherence tomography measurements in glaucoma. *JAMA Ophthalmol*. 2014;132:396–402.
9. Liu Y, Simavli H, Que C, et al. Patient characteristics associated with artifacts in spectralis optical coherence tomography imaging of the retinal nerve fiber layer in glaucoma. *Am J Ophthalmol*. 2015;159:565–576.
10. Leung CK-S, Mohamed S, Leung KS, et al. Retinal nerve fiber layer measurements in myopia: an optical coherence tomography study. *Invest Ophthalmol Vis Sci*. 2006;47:5171–5176.
11. Rauscher FM, Sekhon N, Feuer WJ, et al. Myopia affects retinal nerve fiber layer measurements as determined by optical coherence tomography. *J Glaucoma*. 2009;18:501–505.
12. Mohammad Salih PA-K. Evaluation of peripapillary retinal nerve fiber layer thickness in myopic eyes by spectral-domain optical coherence tomography. *J Glaucoma*. 2012;21:41–44.
13. Zhao J-J, Zhuang W-J, Yang X-Q, et al. Peripapillary retinal nerve fiber layer thickness distribution in Chinese with myopia measured by 3D-optical coherence tomography. *Int J Ophthalmol*. 2013;6:626–631.
14. Savini G, Barboni P, Parisi V, et al. The influence of axial length on retinal nerve fibre layer thickness and optic-disc size measurements by spectral-domain OCT. *Br J Ophthalmol*. 2012;96:57–61.
15. Kim SY, Park H-YL, Park CK. The effects of peripapillary atrophy on the diagnostic ability of Stratus and Cirrus OCT in the analysis of optic nerve head parameters and disc size. *Invest Ophthalmol Vis Sci*. 2012;53:4475–4484.
16. Lai E, Wollstein G, Price LL, et al. Optical coherence tomography disc assessment in optic nerves with peripapillary atrophy. *Ophthalmic Surg Lasers Imaging*. 2003;34:498–504.
17. Leal-Fonseca M, Rebolleda G, Oblanca N, et al. A comparison of false positives in retinal nerve fiber layer, optic nerve head and macular ganglion cell-inner plexiform layer from two spectral-domain optical coherence tomography devices. *Graefes Arch Clin Exp Ophthalmol*. 2014;252:321–330.
18. van der Schoot J, Vermeer KA, de Boer JF, et al. The effect of glaucoma on the optical attenuation coefficient of the retinal nerve fiber layer in spectral domain optical coherence tomography images. *Invest Ophthalmol Vis Sci*. 2012;53:2424–2430.
19. Thepass G, Lemij HG, Vermeer KA. Attenuation Coefficients From SD-OCT Data: Structural Information Beyond Morphology on RNFL Integrity in Glaucoma. *J Glaucoma*. 2017;26:1001–1009.
20. Simavli H, Que CJ, Akduman M, et al. Diagnostic capability of peripapillary retinal thickness in glaucoma using 3D volume scans. *Am J Ophthalmol*. 2015;159:545–556.


 

21. Asrani S, Edghill B, Gupta Y, et al. Optical coherence tomography errors in glaucoma. *J Glaucoma*. 2010;19:237–242.
22. Simavli H, Poon LY-C, Que CJ, et al. Diagnostic capability of peripapillary retinal volume measurements in glaucoma. *J Glaucoma*. 2017;26:592–601.
23. Tah V, Keane PA, Esposti SD, et al. Repeatability of retinal thickness and volume metrics in neovascular age-related macular degeneration using the Topcon 3DOCT-1000. *Indian J Ophthalmol*. 2014;62:941–948.
24. Andreoli MT, Lim JI. Optical coherence tomography retinal thickness and volume measurements in X-linked retinoschisis. *Am J Ophthalmol*. 2014;158:567–573.e2.
25. Gordon MO, Kass MA. The Ocular Hypertension Treatment Study: design and baseline description of the participants. *Arch Ophthalmol*. 1999;117:573–583.
26. Cense B, Nassif N, Chen T, et al. Ultrahigh-resolution high-speed retinal imaging using spectral-domain optical coherence tomography. *Opt Express*. 2004;12:2435–2447.
27. Chen TC, Cense B, Pierce MC, et al. Spectral domain optical coherence tomography: ultra-high speed, ultra-high resolution ophthalmic imaging. *Arch Ophthalmol*. 2005;123:1715–1720.
28. Wu H, de Boer JF, Chen TC. Reproducibility of retinal nerve fiber layer thickness measurements using spectral domain optical coherence tomography. *J Glaucoma*. 2011;20:470–476.
29. Leite MT, Rao HL, Zangwill LM, et al. Comparison of the diagnostic accuracies of the Spectralis, Cirrus, and RTVue optical coherence tomography devices in glaucoma. *Ophthalmology*. 2011;118:1334–1339.
30. Lee EJ, Lee KM, Kim H, et al. Glaucoma diagnostic ability of the new circumpapillary retinal nerve fiber layer thickness analysis based on Bruch's membrane opening. *Invest Ophthalmol Vis Sci*. 2016;57:4194–4204.
31. Schweitzer C, Korobelnik J-F, Le Goff M, et al. Diagnostic performance of peripapillary retinal nerve fiber layer thickness for detection of glaucoma in an elderly population: the ALIENOR Study. *Invest Ophthalmol Vis Sci*. 2016;57:5882–5891.
32. Staurenghi G, Sadda S, Chakravarthy U, et al. International Nomenclature for Optical Coherence Tomography (IN.OCT) Panel. Proposed lexicon for anatomic landmarks in normal posterior segment spectral-domain optical coherence tomography: IN.OCT consensus. *Ophthalmology*. 2014;121:1572–1578.
33. Benjamini Y, Hochberg Y. Controlling the false discovery rate: a practical and powerful approach to multiple testing. *Journal of the Royal Statistical Society. Series B (Methodological)*. 1995;57:289–300.
34. Yi K, Mujat M, Sun W, et al. Peripapillary retinal thickness maps in the evaluation of glaucoma patients: a novel concept. *ISRN Ophthalmol*. 2011;2011:146813.
35. Schuman JS, Pedut-Kloizman T, Hertzmark E, et al. Reproducibility of nerve fiber layer thickness measurements using optical coherence tomography. *Ophthalmology*. 1996;103:1889–1898.
36. Tuulonen A, Airaksinen PJ. Initial glaucomatous optic disk and retinal nerve fiber layer abnormalities and their progression. *Am J Ophthalmol*. 1991;111:485–490.
37. Quigley HA. Early detection of glaucomatous damage. II. Changes in the appearance of the optic disk. *Surv Ophthalmol*. 1985;30:111; 117–126.
38. Pederson JE, Anderson DR. The mode of progressive disc cupping in ocular hypertension and glaucoma. *Arch Ophthalmol*. 1980;98:490–495.
39. Jonas JB, Fernández MC, Stürmer J. Pattern of glaucomatous neuroretinal rim loss. *Ophthalmology*. 1993;100:63–68.
40. Chen TC, Hoguet A, Junk AK, et al. Spectral-domain OCT: helping the clinician diagnose glaucoma: a report by the American Academy of Ophthalmology. *Ophthalmology*. 2018;125:1817–1827.
41. Jonas JB, Gusek GC, Naumann GO. Optic disc, cup and neuroretinal rim size, configuration and correlations in normal eyes. *Invest Ophthalmol Vis Sci*. 1988;29:1151–1158.
42. Tsikata E, Lee R, Shieh E, et al. Comprehensive three-dimensional analysis of the neuroretinal rim in glaucoma using high-density spectral-domain optical coherence tomography volume scans. *Invest Ophthalmol Vis Sci*. 2016;57:5498–5508.
43. Shieh E, Lee R, Que C, et al. Diagnostic performance of a novel three-dimensional neuroretinal rim parameter for glaucoma using high-density volume scans. *Am J Ophthalmol*. 2016;169:168–178.
44. Choi JA, Park H-YL, Jung K-I, et al. Difference in the properties of retinal nerve fiber layer defect between superior and inferior visual field loss in glaucoma. *Invest Ophthalmol Vis Sci*. 2013;54:6982–6990.
45. Jonas JB, Mardin CY, Schlötzer-Schrehardt U, et al. Morphometry of the human lamina cribrosa surface. *Invest Ophthalmol Vis Sci*. 1991;32:401–405.
46. Hood DC, Raza AS, de Moraes CGV, et al. The nature of macular damage in glaucoma as revealed by averaging optical coherence tomography data. *Transl Vis Sci Technol*. 2012;1:3.
47. Chauhan BC, Mikelberg FS, Balaszi AG, et al. Canadian Glaucoma Study: 2. risk factors for the progression of open-angle glaucoma. *Arch Ophthalmol Chic Ill 1960*. 2008;126:1030–1036.
48. Leske MC, Heijl A, Hyman L, et al. Predictors of long-term progression in the early manifest glaucoma trial. *Ophthalmology*. 2007;114:1965–1972.
49. Mukesh BN, McCarty CA, Rait JL, et al. Five-year incidence of open-angle glaucoma: the visual impairment project. *Ophthalmology*. 2002;109:1047–1051.
50. Han IC, Jaffe GJ. Evaluation of artifacts associated with macular spectral-domain optical coherence tomography. *Ophthalmology*. 2010;117:1177–1189.e4.
51. Mansberger SL, Menda SA, Fortune BA, et al. Automated segmentation errors when using optical coherence tomography to measure retinal nerve fiber layer thickness in glaucoma. *Am J Ophthalmol*. 2017;174:1–8.
52. Medeiros FA, Ng D, Zangwill LM, et al. The effects of study design and spectrum bias on the evaluation of diagnostic accuracy of confocal scanning laser ophthalmoscopy in glaucoma. *Invest Ophthalmol Vis Sci*. 2007;48:214–222.


 